Biochimica et Biophysica Acta 1847 (2015) 98–108

Contents lists available at ScienceDirect

Biochimica et Biophysica Acta

journal homepage: www.elsevier.com/locate/bbabio

Review

Proton translocation in cytochrome *c* oxidase: Insights from proton exchange kinetics and vibrational spectroscopy☆

Izumi Ishigami [1], Masahide Hikita [1], Tsuyoshi Egawa, Syun-Ru Yeh, Denis L. Rousseau *

Department of Physiology and Biophysics, Albert Einstein College of Medicine, Bronx, NY 10461, USA

ARTICLE INFO

Article history:
Received 1 July 2014
Received in revised form 11 September 2014
Accepted 20 September 2014
Available online 28 September 2014

Keywords:
Raman spectroscopy
Proton translocation
Cytochrome oxidase
Vibrational spectroscopy
Heme

ABSTRACT

Cytochrome *c* oxidase is the terminal enzyme in the electron transfer chain. It reduces oxygen to water and harnesses the released energy to translocate protons across the inner mitochondrial membrane. The mechanism by which the oxygen chemistry is coupled to proton translocation is not yet resolved owing to the difficulty of monitoring dynamic proton transfer events. Here we summarize several postulated mechanisms for proton translocation, which have been supported by a variety of vibrational spectroscopic studies. We recently proposed a proton translocation model involving proton accessibility to the regions near the propionate groups of the heme *a* and heme a_3 redox centers of the enzyme based by hydrogen/deuterium (H/D) exchange Raman scattering studies (Egawa et al., PLoS ONE 2013). To advance our understanding of this model and to refine the proton accessibility to the hemes, the H/D exchange dependence of the heme propionate group vibrational modes on temperature and pH was measured. The H/D exchange detected at the propionate groups of heme a_3 takes place within a few seconds under all conditions. In contrast, that detected at the heme *a* propionates occurs in the oxidized but not the reduced enzyme and the H/D exchange is pH-dependent with a pK_a of ~8.0 (faster at high pH). Analysis of the thermodynamic parameters revealed that, as the pH is varied, entropy/enthalpy compensation held the free energy of activation in a narrow range. The redox dependence of the possible proton pathways to the heme groups is discussed. This article is part of a Special Issue entitled: Vibrational spectroscopies and bioenergetic systems.

1. Introduction

Cytochrome *c* oxidase (C*c*O), the terminal enzyme of the respiratory chain in mitochondria, reduces dioxygen to water and harnesses the redox energy to translocate protons across the inner mitochondrial membrane. The generated electrochemical potential is utilized for the synthesis of ATP by F_oF_1 ATP synthase. C*c*O has four redox-active metal centers, Cu_A, heme *a*, heme a_3 and Cu_B [1]. Cu_A accepts electrons from cytochrome *c* and transfers them *via* heme *a* to the heme a_3–Cu_B binuclear center where the four-electron reduction of dioxygen to water takes place. Eight protons are taken up from the negative side (N-side) of the mitochondrial membrane; four of those are transferred to the binuclear center for the formation of water and four others are translocated across the membrane to the positive side (P-side). Three proton pathways (H, D and K, named after their entry residue) have been identified and heavily studied. In bacterial aa_3 enzymes the K-channel was shown to supply chemical protons to the binuclear center, while the D-channel was reported not only to supply chemical protons to the binuclear center, but also to serve as the pathway for all four of the translocated protons [2]. In contrast, in bovine C*c*O (bC*c*O), proton translocation has been attributed to the H-channel, which passes near heme *a* [3].

Although the proton conducting channels have been identified, the molecular mechanism for the proton translocation remains unresolved. Indeed, whether or not aa_3 enzymes from bacteria and bovine have different mechanisms of proton translocation remains an open question. This is a result of the difficulty of identifying protonation states of critical residues within the large membrane bound enzyme during its catalytic turnover, although some labile positions have been identified under equilibrium or quasi-equilibrium conditions by vibrational spectroscopy [4–17] and some have been postulated by electrostatic calculations [18–21]. Such studies have led to new insights into proposed mechanisms of proton translocation, some of which are discussed below.

Infrared absorption and resonance Raman spectroscopies have been extensively used with great success to study the properties of terminal

Abbreviations: bC*c*O, bovine Cytochrome *c* Oxidase; $[[CcO^{Ox}{}_D]_{H,t\ min}]^{Rd}$, treatment order of the enzyme, the oxidized (Ox) was treated in deuterated buffer (D) for at least 8 h, the buffer was exchanged for a protonated buffer (H) and incubated for t minutes before reduction (Rd); N-side and P-side, the negative and positive sides of the mitochondrial membrane, respectively

☆ This article is part of a Special Issue entitled: Vibrational spectroscopies and bioenergetic systems.

* Corresponding author. Tel.: +1 718 430 4264.
E-mail address: rousseau@aecom.yu.edu (D.L. Rousseau).

[1] Authors contributed equally to this work.

http://dx.doi.org/10.1016/j.bbabio.2014.09.008
0005-2728/

oxidases. In general, the two techniques have yielded complementary information. The infrared spectrum reports on functional groups of the protein provided that there are changes in the dipole moment associated with their vibrational modes. As a result, the spectra tend to be complicated with overlapping features. In addition, the infrared spectrum can be obscured by the strong IR bands from water molecules, especially the water bending mode that occurs in the 1600 cm^{-1} region of the spectrum which overlaps with the Amide-I mode of the protein matrix as well as modes from sidechains from several types of amino acids. Various techniques have been used to address this problem. For instance, attenuated total reflection (ATR), in which a sample in contact with the ATR crystal is probed by the evanescent wave, makes the water pathlength short enough to reduce its contribution to the spectrum [6,22,23]. A new technique, reviewed in this issue by Nakashima, et al., uses a very intense IR laser beam to penetrate the water matrix surrounding the protein sample [17,24]. Difference spectra e.g. oxidized minus reduced [11], or CO-bound *versus* CO-photodissociated [13,14], are used to identify features in the infrared spectrum that may be functionally important.

In contrast to infrared absorption spectroscopy, resonance Raman scattering reports on those moieties with an optical transition which coincides with the excitation wavelength. Consequently, with visible excitation overlapping with the heme absorption bands, the resonance Raman spectrum probes the heme groups selectively, without spectral interference from the surrounding protein. The resonance Raman spectrum is sensitive to the electronic properties of the heme and perturbations of it induced by the protein environment. The contribution of water is relatively weak in the Raman spectrum, so it generally is not a factor in determining the quality of the spectrum. There is a great deal of information in the resonance Raman spectrum of the heme group, such as the redox and spin state of the iron atom, and the conformational properties of the heme macrocycle, as well as the peripheral groups attached to it. In addition, due to its strong scattering intensity, the resonance Raman spectrum of the heme can be obtained at relatively low sample concentrations; hence, it can be easily coupled with continuous-flow cells for time-resolved measurements, without excessive sample consumption, allowing determination of catalytic intermediates by time resolved techniques [25,26].

2. The catalytic reaction of C*c*O

To translocate protons against an electrochemical gradient, energy has to be supplied to the system. For terminal oxidases, energy is supplied by the reduction of oxygen to water at the binuclear center, a process that involves several intermediates, which have been well-characterized by resonance Raman studies [27–32]. The catalytic cycle, illustrated in Fig. 1, shows the stretching modes of the oxygen intermediates that were determined by time-resolved experiments carried out primarily by three different groups using either continuous-flow or pulsed laser spectroscopic techniques [29,31,32]. In the continuous-flow procedure, the CO-inhibited reduced enzyme is mixed with oxygen and flowed into an observation cell, where one laser beam photodissociates the CO, allowing the O_2 to bind to the enzyme, and a second laser, downstream from the photolysis beam, excites the Raman spectrum [25]. The reaction time at a given probe position is determined by the flow rate and the separation between the two laser beams. The signal to noise ratio of the Raman spectrum is determined by the spectral integration time at a given position. In the pulsed experiments, the CO-bound enzyme, mixed with O_2, is loaded into the observation cell, where a laser pulse photodissociates the CO and a second laser pulse, time delayed from the first, excites Raman spectrum [33,34]. Subsequently, a new sample is loaded into the observation cell and the process is repeated a number of times until a spectrum with a satisfactory signal to noise ratio is obtained. The reaction time is given by the time delay between the two laser pulses.

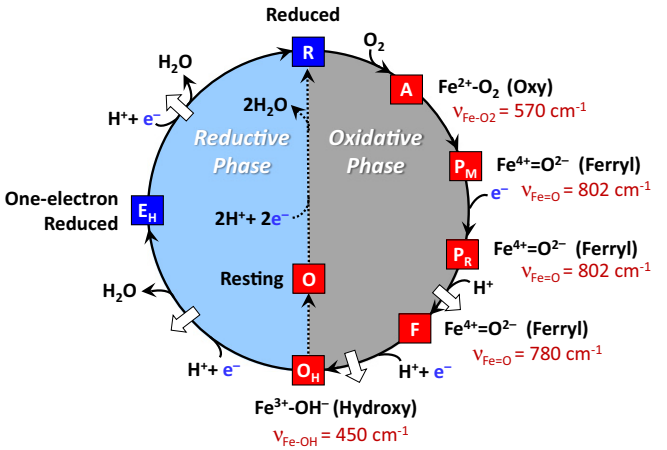

Fig. 1. The redox cycle of cytochrome *c* oxidase. The white arrows designate the proposed proton translocation events. If, after the $\mathbf{O_H}$ species is formed, the enzyme is rapidly reduced, it passes through $\mathbf{E_H}$ on its way to the reduced state, **R**, and two protons are translocated. However, if the reduction does not occur immediately, the resting oxidized species (**O**) is formed, and no proton translocation is associated with its reduction to the **R** species. The characteristic vibrational mode associated with each oxygen intermediate is indicated in red.

Raman measurements led to the firm determination of the identity of the catalytic intermediates. In the initial O_2-bound species (the **A** intermediate), the Fe – O_2 stretching mode was identified at 570 cm^{-1}, the same as that found in myoglobin, indicating that the nearby Cu_B does not significantly perturb the Fe-O_2 moiety [35,36]. The identification [37] of the Fe═O mode of the **P** intermediates at 802 cm^{-1} is particularly interesting as initially the **P** intermediate was thought to be a peroxy species. However, resonance Raman studies of a **P** analog derived from the H_2O_2 reaction with C*c*O, carried out by Kitagawa and coworkers, demonstrated that the species had only one oxygen atom, proving that it was a ferryl rather than a peroxy species [37]. This assignment was subsequently confirmed by biochemical [38] and other spectroscopic measurements [39]. In addition, the structure of the intermediate was confirmed by additional resonance Raman measurements of the catalytic reaction [31,40,41]. In the **F** intermediate, another ferryl species was detected, in which the Fe═O stretching mode was identified at 780 cm^{-1} by several groups [28–30,42]. Although both **P** and **F** are ferryl species, they differ by one redox equivalent with **P** having an additional oxidation equivalent, the location of which is under constant debate. Presumably, they also differ by the ligand coordinated to Cu_B, likely a hydroxide in **P** and a water molecule in **F** [2]. Finally, the $\mathbf{O_H}$ species was shown to be a hydroxide-bound high-spin intermediate with a Fe – OH stretching mode at 450 cm^{-1} [28]. The Fe – OH stretching frequency is very low with respect to other hydroxide bound heme species; we attribute this very low frequency to the presence of a strong H-bond to the oxygen atom, thereby weakening the Fe – O bond and generating a high-spin configuration.

3. Postulated proton pumping mechanisms

Although the properties of the catalytic intermediates are reasonably well-understood, how the oxygen reduction reaction leads to the concerted conformational changes and electrostatic processes that drive protons across a membrane against a proton gradient remains to be determined. Maintaining charge neutrality at the metal centers as electrons and protons flow through the protein during the redox processes is a critical component in coupling oxygen reduction to proton translocation [43]. Schematically, for proton translocation to occur efficiently, a proton loading site with two gates, where protons can be stored and released in a controllable fashion, is needed. In principle, the loading site can have a variable pK_a, which is regulated by the redox and ligand binding states of the heme group. Under conditions

of high pK_a a proton is accepted *via* a channel with an open gate from the N-side of the membrane. Subsequently, the gate on the input channel closes, a conformational change lowers the pK_a of the loading site, and the gate in the output channel, connected to the P-side of the membrane, opens allowing the release of the proton. This is of course an over-simplified picture as directional proton movements are not only regulated by conformational changes of gates, but can be regulated by electrostatic changes [18] and rectified by kinetic barriers [19,44]. Postulated mechanisms of proton translocation, considered within this framework, have been evaluated by vibrational spectroscopy, which has played an important role in probing possible gates, monitoring conformational changes and identifying putative loading sites.

3.1. E242 diverter valve mechanism

Many studies on bacterial heme-copper oxidases, especially those from *Rhodobacter sphaeroides*, *Escherichia coli* and *Paracoccus denitrificans*, have led to models in which protons are translocated *via* the D-channel terminating at E242 (bovine numbering is used throughout) [45–48]. It is believed that E242 can serve as both a diverter valve and a gate, as conformational changes in its side chain can either divert the protons to the binuclear center, to be used for the formation of water, or it can pass the protons to the putative loading site associated with the heme a_3 propionates (Fig. 2) [18,49–51]. Although the details vary, several models for proton translocation, based on the passage of protons through E242, have been put forth [2,19,20,44–46,50–59].

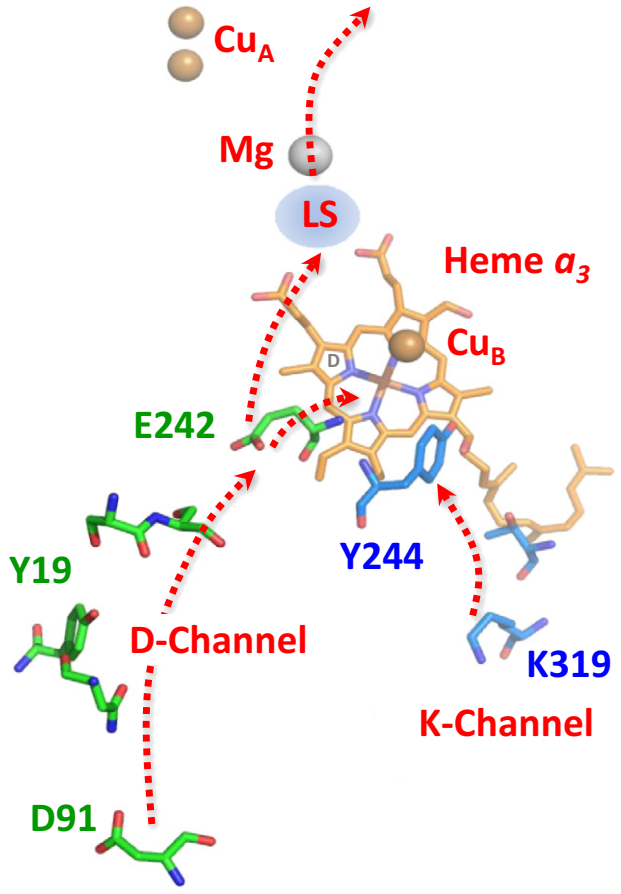

Fig. 2. The D and K proton translocation channels. The D-channel starts at D91 and ends at E242, which serves as a diverter valve, transferring protons to either the binuclear center for the reduction of O_2 to water or to the proton loading site (LS) for subsequent translocation of protons to the P-side of the membrane. All structures depicted in this paper were made with PyMol Molecular Graphics Software (Delano Scientific, LLC).

It has been proposed, based on MD calculations, that when heme *a* accepts an electron, the A-ring propionate of heme a_3 rotates into an open conformation, increasing its pK_a, allowing it to accept a proton from E242 *via* the D-ring propionate of heme a_3, due to a change in its H-bonding interactions [18,45]. The proton is "loaded" in this region of the protein until it is subsequently ejected to the P-side of the membrane due to changes in the electrostatic environment at the heme a_3 site. It has been postulated that for this model to be viable backflow of protons from the P-side of the membrane to the loading site has to be prohibited and specific gates have been proposed [50]. However, it has also been postulated that a molecular gate is unnecessary as the backflow can be prevented by kinetic barriers [19].

Vibrational spectroscopy has been very powerful in providing evidence for structural changes in the key residues associated with the E242 diverter valve mechanism, considering the fact that structural changes in residues postulated to be critical for proton translocation have not been detected in static structures probed by X-ray crystallographic studies. Especially important are the many studies that have been carried out on E242 and the equivalent residues in bacterial oxidases. Conformational changes in E242 were first reported by Hellwig et al. in 1996, in which FTIR difference spectra were obtained from *P. denitrificans* *Cc*O, which was electrochemically reduced and oxidized [60]. The C═O stretching modes were detected at 1733 and 1745 cm^{-1} in the reduced and oxidized states, respectively, although at that time assignment to a specific residue could not be made. Subsequently, by mutagenesis studies, the modes were assigned as originating from the carboxylate side chains of E278 (equivalent to E242 in bovine), indicating a change in its environment upon reduction [61]. Independently, Puustinen et al. measured the properties of the modes of the equivalent residue (E286) in cytochrome bo_3 from *E. coli*, by generating the difference spectrum formed by photodissociating carbon monoxide (CO) from heme o_3, which then binds to Cu_B [62]. The C═O stretching mode of the E286 sidechain shifted from 1726 to 1730 cm^{-1} when the CO moved from the o_3 iron atom to the Cu_B, indicating that the sidechain conformation of E286 is sensitive to the ligation state of the heme o_3. The assignment of the C═O stretching mode to E286 was confirmed by mutagenesis.

Subsequent to the initial assignments of the E242 mode and its equivalent in the *P. denitrificans* and *E. coli* enzymes, studies of these modes in various metastable states of the enzyme were carried out by a variety of techniques, including CO-photolysis [13,14], as well as O_2, CO and H_2O_2 perfusion [22,63]. Based on these studies, the difference spectra of several different forms of oxidase were reported including: i) CO-bound minus CO-photodissociated, ii) oxidized minus fully reduced [11], iii) intermediate **E** (see Fig. 1) minus two electron reduced CO-bound [13], iv) intermediate $\mathbf{P_M}$ minus oxidized [12] and v) intermediate **F** minus oxidized (**O**) [63]. All of the studies led to the similar conclusion that E242 undergoes conformational changes and, in a few cases deprotonation, in response to the changes in the oxidation and/or ligation states of the metal centers. However, there were significant differences among the various oxidases, as summarized by Iwaki and Rich [64]. Bovine *Cc*O only became deprotonated when intermediate **E** was generated by CO-photolysis of the 2-electron reduced CO-bound enzyme [13]. A similar change was observed in the *R. sphaeroides* enzyme [63]. It should be noted that intermediate **E** is generated by the CO-photolysis of the 2-electron reduced enzyme (reduced heme a_3 and Cu_B), where subsequent to the photolysis reverse electron transfer takes place (to heme *a*), leaving only one electron on the heme a_3–Cu_B binuclear center. For *R. sphaeroides*, in addition to being deprotonated in intermediate **E**, the glutamate residue was deprotonated in the $\mathbf{P_M}$ intermediate [63]. For all of the other cases the carboxyl mode of E242, or its equivalent, was either unaffected or slightly perturbed. These data clearly demonstrated the sensitivity of E242 to the changes in the redox and ligation states of the metal centers,

but they did not reveal a clear mechanistic support for the E242 diverter valve mechanism. In fact, recently, it has been proposed that E242 is not a gating element in oxidases [65]. Clearly experiments to detect the temporal changes in the C═O (carboxylate) stretching mode of E242 during the catalytic reaction are highly desirable to resolve these issues.

3.2. Tyrosine radical mechanism

Vibrational spectroscopy has clearly shown that, when H_2O_2 reacts with oxidized oxidase, a ferryl species (**P** or **F**) is formed [37,66,67]. As an insufficient number of electrons from H_2O_2 and the metal centers are available to cleave the O – O bond and form the $\mathbf{P_M}$ ferryl intermediate, it has been postulated [40] that an additional electron is supplied from an amino acid residue, presumably a tyrosine (Y244). The Y244 residue is covalently linked to a Cu_B histidine ligand due to a posttranslational modification. Recently, it was demonstrated by optical absorption and by low and high field EPR spectroscopy (in which the hyperfine splitting and the g values were determined) that the electron indeed was supplied from Y244, leaving a radical on it, which migrated to Y129 as the $\mathbf{P_M}$ intermediate decayed to the **F** intermediate [66,67]. This led to a proton translocation model based on radical formation and migration as illustrated in Fig. 3 [66].

In the postulated model [66], in the formation of the $\mathbf{P_M}$ state, one electron is transferred from Y244 to the iron-oxygen moiety to cleave the O – O bond, leaving a radical center on Y244. This $\mathbf{P_M}$ species decays to the **F** intermediate, associated with radical migration to Y129 (*i.e.* an electron is transferred from Y129 to reduce Y244), leaving a radical on Y129. Concomitant with the electron transfer, a proton is also ejected to generate a neutral radical on Y129.

$$\text{Y129–OH} \leftrightarrows \text{Y129–O}^{\bullet} + e^{-} + H^{+} \quad (1)$$

As the putative proton loading site (Y129) and the water molecules leading to it from the hemes are fully loaded, the proton is ejected to the P-side of the membrane. Y244, which is on the N-side of the hemes, then picks up a proton from the K or D channel to maintain its charge neutrality. The radical on Y129 is reduced when an electron from heme *a* transfers to it while it picks up a proton from the nearby water molecule, which, as shown in Fig. 3, is only 2.8 Å from the tyrosine oxygen atom thereby completing the formation of the **F** intermediate, and resetting the loading site. An electron is transferred from Y244 to the binuclear center for the next step of the oxygen reduction to occur. On the basis of this model, Y129 can be considered as part of the putative proton loading site that contributes to the gating of proton translocation.

3.3. Cu_B–S382 relay mechanism

Very recently Yoshikawa and coworkers proposed a new mechanism for proton translocation based on a combination of time-resolved

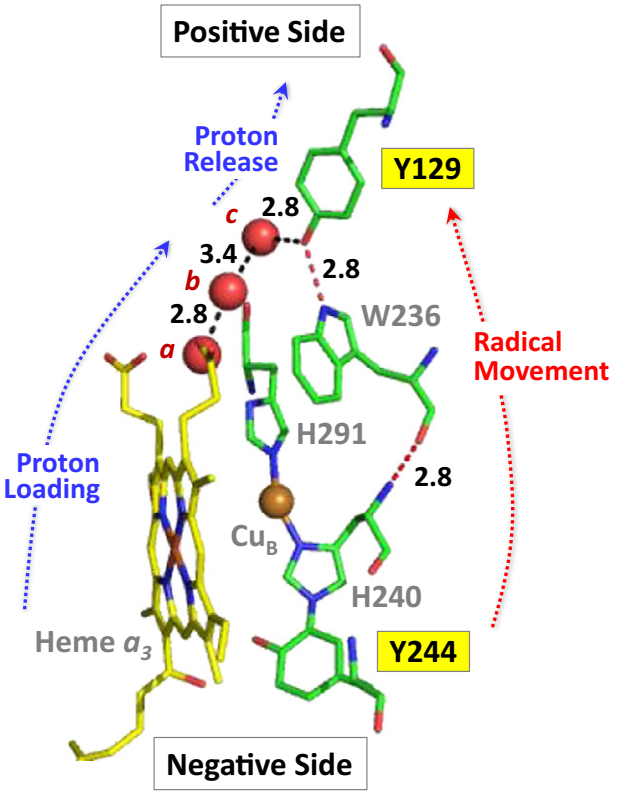

Fig. 3. Structure of the heme a_3–Cu_B binuclear center, and Y244 and Y129, in bCcO (PDB ID: 3AG3) with respect to the positive and negative sides of the inner mitochondrial membrane [66]. The three water molecules, indicated by the red spheres are part of the water cluster near the heme a_3 propionates. These three water molecules directly link the propionates of heme a_3 to Tyr-129 by a H-bonding network (black dashed lines). The radical migration between Y244 and Y129 may occur through the Y244–H240–W236–Y129 network linked by H-bonds. The H-bond distances (in Å) between water molecules a, b and c and that between c and the oxygen of Y129 are indicated.

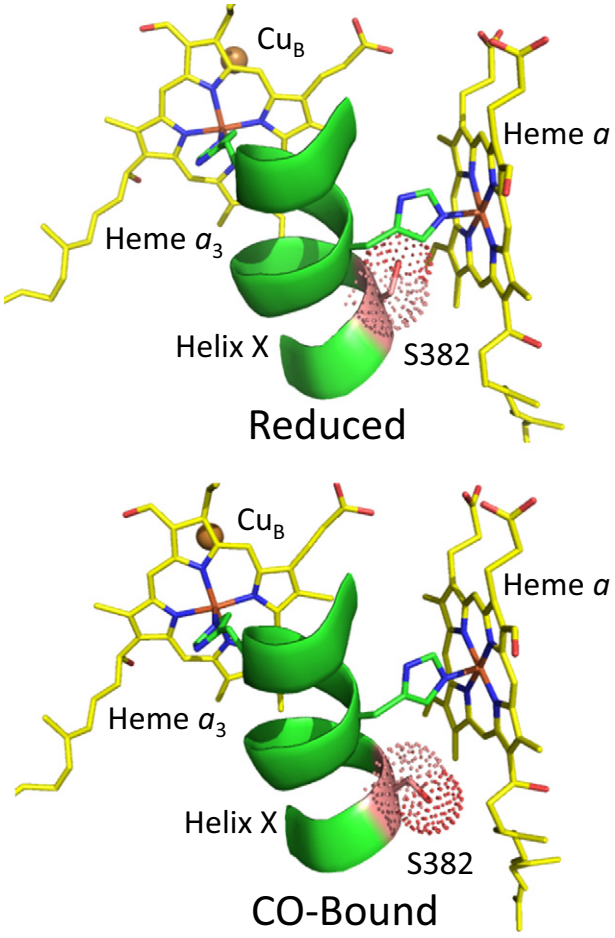

Fig. 4. Comparison of the conformation of S382 in reduced (PDB ID: 2EIJ) *versus* CO-bound (PDB ID: 3AG2) bCcO. In the CO-bound form, the sidechain of S382 occludes a water channel located near heme *a*; the change in the orientation of the sidechain channel in the reduced form leads to the opening of the channel.

infrared absorption, time-resolved resonance Raman scattering and crystallographic studies of bCcO [17]. Using their newly developed time-resolved IR spectrometer they identified changes induced by CO-photodissociation in the Amide-I mode region (1655–1666 cm^{-1}). This was interpreted as changes in the helical structure in the V380 to S382 section of the protein based on comparisons of the crystal structures of the ligand-free and CO-bound reduced enzyme, in which a bulge in Helix-X in the V380 to S382 residue region was noted. As may be seen in the structures shown in Fig. 4, the sidechain of S382 may be oriented in two different directions. In the CO-bound enzyme, S382 is oriented into the region below heme *a* blocking the water channel, which was previously identified by Yoshikawa and coworkers [3]. However, in the ligand-free reduced enzyme the orientation of S382 changes so as to open the water channel. It is notable that following photodissociation of the CO from the heme iron atom, the CO binds to Cu_B and spontaneously dissociates from it on a 1 μs time scale [17,68]. The time of the changes in the Amide-I mode correlates well with the dissociation of the CO from Cu_B, which was also measured in the IR absorption spectrum.

Based on these observations, a Cu_B–S382 relay mechanism was postulated [17]. When O_2 enters the enzyme, it binds to Cu_B, which induces a change in the size and proton affinity of the water cavity near S382 resulting in the uptake of a proton. Owing to a relay between Cu_B and S382, this proton uptake causes the release of the O_2 without binding to the heme a_3 iron. The proton is then passed to a loading site resetting the protein, allowing it to bind O_2 again. This process is repeated 4 times. The loading of 4 protons in the proton loading site enables the next O_2 bound to Cu_B to transfer to the heme a_3, thereby initiating the oxygen reduction reaction. The gate to the N-side of the membrane is closed whenever a ligand is coordinated to the iron atom, in analogy to the CO results described above. Subsequently, during the electron transfer steps associated with the redox cycling, the protons are sequentially pumped to the P-side of the membrane as they cannot slip backwards since the gate remains closed.

3.4. Heme a redox-gate mechanism

Recently, in an effort to determine proton accessibility to various regions of the enzyme, Egawa et al. carried out a series of hydrogen/deuterium (H/D) exchange experiments in bCcO with resonance Raman spectroscopy [5]. It was discovered that protons were rapidly accessible to the region near the propionate groups of heme a_3. However, protons were inaccessible to the propionates of heme *a* in the reduced form of the enzyme but were accessible in the oxidized form. Consideration of these results, combined with the reported crystal structural data, suggests that entry to a proton loading site from the N-side of the membrane is gated by conformational changes of the R38-formyl group of heme *a* and a nearly 180° rotation of the OH group of the farnesyl side chain; while from the P-side, proton movement is gated by an keto-enol transition [69,70]. The crystal structures of these regions are shown in Fig 5. As shown in Fig. 5A, the A-ring propionate group of heme *a* forms a H-bond with a water molecule, which in turn is H-bonded to the backbone carbonyl groups of Y440; the adjacent backbone amine group of S441 is H-bonded to D51. These backbone groups have been postulated to undergo a keto-enol tautomerization [69,70]. In Fig. 5B, the near 180° rotation of the OH of the farnesyl side chain of heme *a* induced by reduction is illustrated. Associated with this change, S382 also undergoes a large conformational change. Based on the spectroscopic and crystallographic results, a postulated model for proton translocation *via* the H-channel was proposed [5]. It should be noted that, although this model is based on proton translocation *via* the H-channel, in this redox-gate mechanism, the gate to the loading site is open in the oxidized state and closed in the reduced state, opposite to that proposed in the Cu_B–S382 relay mechanism described above.

As illustrated in the mechanistic model, shown in Fig. 6, in the fully reduced enzyme, **R**, the A-ring propionate (Pr_A) of heme *a* is protonated. Proton accessibility to the region near the heme *a* propionates is blocked from the N-side surface, due to the closed conformation of the heme *a* farnesyl sidechain and the heme *a* formyl-R38 moiety; it is also blocked from the P-side, owing to the keto conformation of the Y440–S441 peptide bond. Accordingly, there is no H/D exchange in the heme *a* site in the equilibrium **R** state.

When heme *a* becomes oxidized, the change in the charge of the heme iron from +2 to +3 triggers the deprotonation of the Pr_A group. It leads to a series of proton transfers from Pr_A to the carbonyl group of Y440, which promotes the keto → enol transition of the Y440–S441 peptide bond and the transfer of a proton to D51 on the P-side of the membrane. The proton movement results in an unstable transient state, designated as $\mathbf{I_1}$, which is associated with a frustrated protein structure that is relaxed to the equilibrium **O** state on a much longer time scale. The conformational wave initiated by the redox change in heme *a* associated with the relaxation process induces the

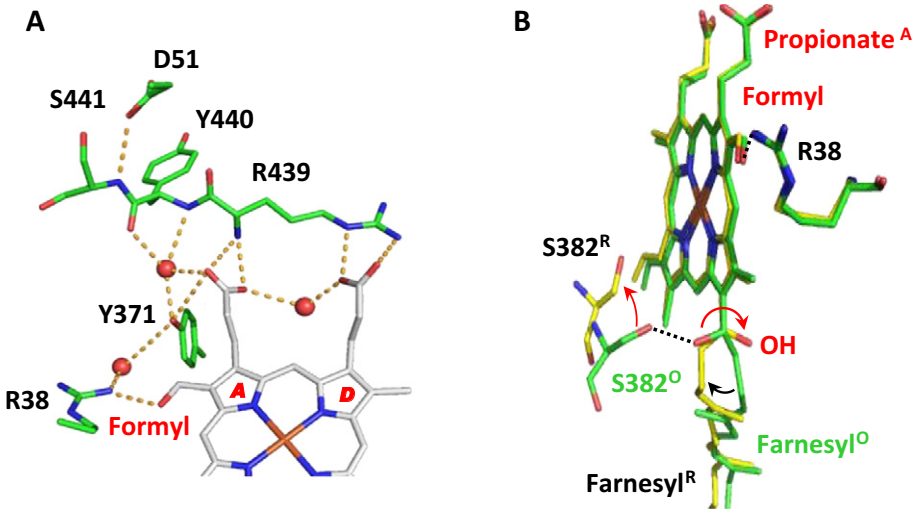

Fig. 5. The structural change of heme *a* induced by reduction [5]. (A) The H-bonding network between the propionate groups of heme *a* and the amino acids/water surrounding it in fully oxidized bCcO (PDB: 3ABL). The red spheres indicate water molecules. (B) The comparison of heme *a* in the fully oxidized enzyme (PDB: 3ABL) and fully reduced enzyme (PDB: 2EIJ), which are highlighted in green and yellow, respectively. The dotted lines indicate the H-bonds present in the fully oxidized state; the red arrows indicate the structural changes induced by heme reduction. The structural alignment was made by superimposing the heme iron atoms.

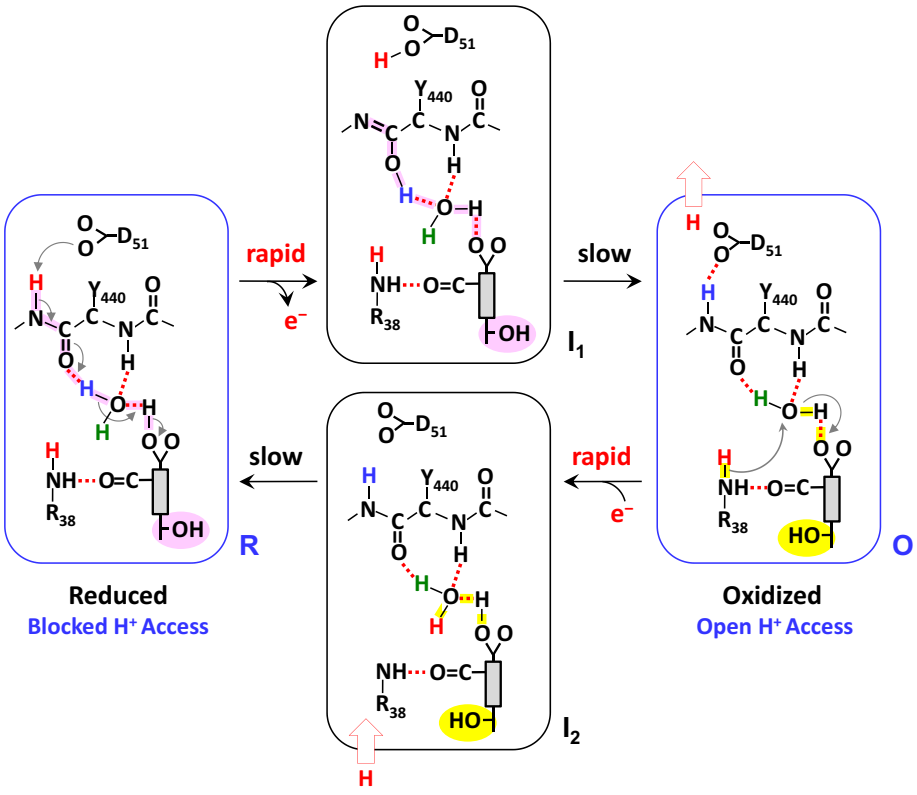

Fig. 6. Mechanistic model for proton translocation in bCcO [5]. The gray rectangular box indicates the heme *a*, with the farnesyl sidechain, formyl and propionate A groups attached to it. The OH group of the farnesyl sidechain in the "open" and "closed" conformations (see text) is highlighted in yellow and pink, respectively.

change of the heme *a* farnesyl sidechain and the heme *a* formyl-R38 moiety from the closed to the open conformation and resets the enol conformation of the Y440–S441 peptide bond back to the more stable keto conformation. The enol → keto transition triggers the rearrangement of the associated H-bonding network, which allows the ejection of a proton to the P-side surface, leaving D51 in a deprotonated state. The new conformation enables proton/water accessibility to the heme *a* site from the N-side surface *via* the H-channel, accounting for the observed H/D exchange in the heme *a* site in the equilibrium **O** state.

When the oxidized heme *a* becomes reduced, the change in the heme iron from +3 to +2 induces the rapid protonation of the Pr_A group, by taking up a proton from the N-side surface as the farnesyl group is in the open conformation. It leads to the transient $\mathbf{I_2}$ state that is subsequently relaxed to the equilibrium **R** state, in which the farnesyl group reverts back to the closed conformation.

The model assumes that the rapid proton rearrangement triggered by the redox state changes in heme *a* precedes the slower conformational change associated with the heme *a* farnesyl sidechain and the heme *a* formyl-R38 moiety. It is hypothesized that the same redox-controlled proton movement takes place during enzymatic turnover, in particular during the **P** → **F**, **F** → **O**, **O** → **E** or **E** → **R** transitions, as during each transition an electron is delivered from cytochrome *c* to the binuclear center *via* heme *a* (*i.e.* each transition is associated with a reduction–oxidation cycle of heme *a*). On the basis of this mechanism, each time an electron passes through heme *a*, a proton is translocated from the N-side surface to the P-side surface; in addition, the proton translocation is controlled by the redox state of heme *a* and is independent of the oxidation and coordination state of the heme a_3.

4. Temperature and pH-dependence of proton exchange in bovine cytochrome *c* oxidase

To further elucidate the heme *a* redox-gate mechanism (Section 3.4), we have measured the temperature and pH dependence of the H/D exchange reactions, from which the apparent pK_a and the thermodynamic parameters associated with the exchange reaction were determined.

4.1. Materials and methods

CcO was isolated as described by Yoshikawa and coworkers [71]. The protein samples were purified in a buffer containing 0.2 M sodium phosphate, pH 7.4, with 0.2% n-decyl-β-maltoside and stored at −80 °C until the H/D exchange treatments. The deuterated buffers were prepared using high purity D_2O (99 atom % D) from Cambridge Isotope Laboratories, Inc. (Andover, MA). The D_2O buffers contained 0.2% n-decyl-β-maltoside and either 0.2 M Tris, pD 8.8, pD 8.3, pD 8.0 or 0.2 M sodium phosphate, pD 7.8, pD 7.3, pD 6.8. The H_2O buffers used had the same concentrations of n-decyl-β-maltoside with either Tris or sodium phosphate. The pH of the Tris buffer was measured at each temperature because the pH of Tris buffers change slightly with temperature. The pD of the D_2O buffers was measured using an ordinary pH meter assuming that the reading of the meter was lower by 0.39 as compared to the pD value. To prepare the fully H to D exchanged samples, the stock CcO solution was diluted into the D_2O buffer at a 1:9 ratio, and the diluted solution was concentrated to ~10% volume using a Millipore concentrator. Repeating this process three times enabled ~99 atom % (98.9% in theory) D in the sample preparations. This sample was then incubated overnight to complete the isotope exchange.

Resonance Raman scattering, from samples in a spinning cell, was excited by the 441.6 nm line of a He–Cd laser (Kimmon Electric,

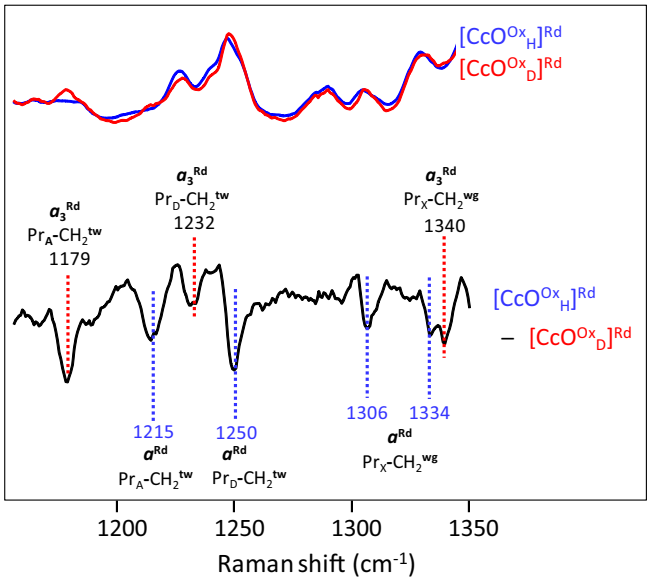

Fig. 7. H_2O/D_2O sensitive propionate Raman bands of heme a^{2+} (a^{Rd}) and heme a_3^{2+} (a_3^{Rd}). Resonance Raman spectra of the fully-reduced form of bCcO in H_2O (blue) and D_2O (red) were obtained with 441.6 nm excitation. The difference spectrum (H_2O–D_2O) (the bottom black trace) is shown with a scale expanded by 3-fold as compared to the parent spectra.

Centennial, CO), and dispersed by a Spex 1.25 m polychromator equipped with a charge-coupled device detector (Princeton Instruments, 1100 PB). The laser power at the sample cell was 10 mW. Optical absorption spectra were measured on a Shimadzu UV2100U spectrophotometer. For the resonance Raman measurements, the dilution experiments were designed so that the final concentration of the CcO samples was 30 μM. Before the experimental measurements, the CcO stock sample (300 μM) and stock buffer were incubated under N_2 gas at each temperature in a water-bath. The gas phase in the Raman cell was replaced by N_2 and after each sample incubation time, $Na_2S_2O_4$ solution was added (final concentration, 6 mM) to reduce the CcO. The resonance Raman intensity from the samples at the same concentration was sometimes slightly different, depending on small changes of the laser power. Therefore, for the spectral difference calculations, we normalized each resonance Raman spectrum on the basis of the ν_4 band intensity, which is the strongest band among the porphyrin core vibrations.

4.2. Results

To monitor the H/D exchange reaction, a reference spectrum was first generated by subtracting the spectrum of the fully deuterium-exchanged sample of bCcO from that of the fully protonated sample. These protonated and deuterated samples were formed by incubating oxidized bCcO in H_2O and D_2O buffers, respectively, for 10 h at 4 °C. To obtain the characteristic difference spectra shown in Fig. 7, the samples were reduced with sodium dithionite under a nitrogen atmosphere prior to the spectral measurements. The samples are labeled as [CcO$^{Ox}_{H}$]Rd and [CcO$^{Ox}_{D}$]Rd in which the order of the treatment is indicated by the superscripts and subscripts. Thus, the superscript (Ox) followed by the subscript (H or D) indicates that the oxidized enzyme was incubated in protonated (H) or deuterated (D) buffers, respectively, and subsequently the samples were reduced (Rd) for the spectral analysis. Fig. 7 shows both the individual spectra of the reduced samples and the difference spectrum.

As was reported previously, the lines in the [CcO$^{Ox}_{H}$]Rd–[CcO$^{Ox}_{D}$]Rd difference spectrum, can be assigned as wagging and twisting modes of the propionate groups of heme *a* or heme a_3 as indicated by the labeling on the spectra [4]. As there are no exchangeable protons on the CH_2 groups of the propionates, the isotope sensitivities of these vibrational modes are ascribed to exchangeable protons residing on the carboxyl groups of the propionates and/or the amino acids/water molecules that form H-bonds with them. The H/D exchange results in conformational changes that induce the small but reproducible changes in the propionate CH_2 modes [4,5]. The negative lines at 1215 and 1250 cm^{-1} are assigned to CH_2 twisting modes of the propionate groups of the A (Pr_A) and D (Pr_D) pyrrole rings of heme *a*, respectively, and the lines at 1306 and 1334 cm^{-1} are assigned to the CH_2 wagging mode of the propionates of heme *a*, which is indicated as Pr_X–CH_2^{wg} (Pr_X stands for either Pr_A or Pr_D), as the specific assignment to each propionate group of heme *a* could not be made [4,5,72,73]. Similarly the lines at 1179, 1232 and 1340 cm^{-1} in the difference spectrum in Fig. 6 may be assigned to modes originating from the propionate groups of heme a_3, although there is a small amount of overlap in some of the modes. It is notable that the same spectral features were obtained from the aa_3 CcOs from *P. denitrificans* and *R. sphaeroides* [4,5].

To determine the time-dependence of the H/D exchange in the oxidized enzyme, an oxidized sample, incubated in deuterated buffer, was placed in protonated buffer for a period of time, t, and then reduced for the spectral measurement, *i.e.* [[CcO$^{Ox}_{D}$]$_{H,\ t\ min}$]Rd. Difference spectra were then obtained with respect to [[CcO$^{Ox}_{D}$]$_{H,\ 0\ min}$]Rd in which the deuterated sample was reduced immediately (a few seconds) after exposure to the protonated buffer. The [[CcO$^{Ox}_{D}$]$_{H,\ 0\ min}$]Rd sample was used as a reference so that the difference spectrum reflects the changes induced by H/D exchange within the designated incubation time, while any exchange that occurred within the mixing dead time cancels out. This is important as we have shown previously that the H/D exchange near the heme a_3 propionates is complete within the mixing dead time; thus, the changes described here only involve those associated with the heme *a* propionates.

A typical set of progressive difference spectra obtained at pH 8.8 and 13 °C is shown in Fig. 8, in which data were obtained from t = 2 min to t = 60 min. The data were simulated by adjusting the amplitude of the reference difference spectrum, [[CcO$^{Ox}_{H}$]$_H$]Rd–[[CcO$^{Ox}_{D}$]$_{H,\ 0\ min}$]Rd, shown at the bottom of Fig. 8. The amplitude factor determined from the simulation was then plotted as a function of the H/D exchange

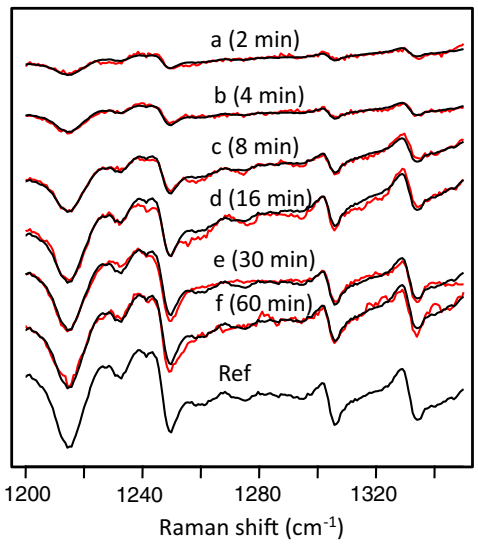

Fig. 8. Time-dependence of the H/D exchange in the oxidized enzyme (red spectra). The data were simulated by adjusting the amplitude of the reference spectrum. The best simulated spectra are shown in black. These data were obtained at pH 8.8 and 13 °C and are typical of the data presented in this work.

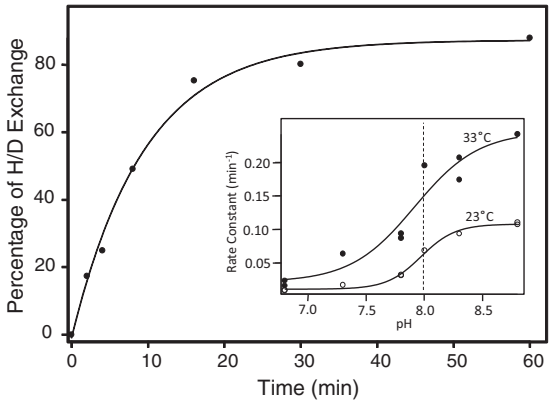

Fig. 9. The percentage of H/D exchange determined from the amplitude factors in Fig. 8 are plotted as a function of the H/D exchange time. The solid line shows the best single exponential fit of the data. The inset shows the rate constants as a function of pH at 23 and 33 °C.

time, as shown in Fig. 9. A single exponential fit of the data gave the rate constants for the H/D exchange reaction at a given pH and temperature. Comparable studies were carried out at pHs ranging from 6.8 to 8.8 and at temperatures from 13 °C to 33 °C. The apparent pk_a was determined to be ~8.0, independent of the temperature (see the insert in Fig. 9).

The same measurements were repeated as a function of temperature from 13 °C to 33 °C at two pH conditions, pH 7.3 and 8.8, and the data were analyzed by using the Eyring equation:

$$\ln(k/T) = \ln(k_B/h) + \Delta S^{\ddagger}/R - \Delta H^{\ddagger}/(RT). \quad (2)$$

The data are plotted in Fig. 10 and the thermodynamic parameters thus obtained are listed in Table 1. Interestingly, the activation enthalpy ($\Delta H^{\ddagger}$) and entropy ($\Delta S^{\ddagger}$) are very different for the reactions carried out at the two pH conditions, but the difference in the activation free energy ($\Delta G^{\ddagger}$), calculated from $\Delta H^{\ddagger}$–$T\Delta S^{\ddagger}$, is relatively small (22.1 *vs* 20.6 kcal mol^{-1}) due to enthalpy/entropy compensation [74].

4.3. Discussion

To obtain insights into mechanisms of proton translocation in CcO, it is necessary to identify potential proton loading sites, where protons can be stored and released during the oxygen reduction cycle. Recently, we identified a labile site, by H/D exchange experiments, near to or associated with the propionate groups of heme *a* in bCcO, based on which a mechanism of proton translocation was postulated [5], as

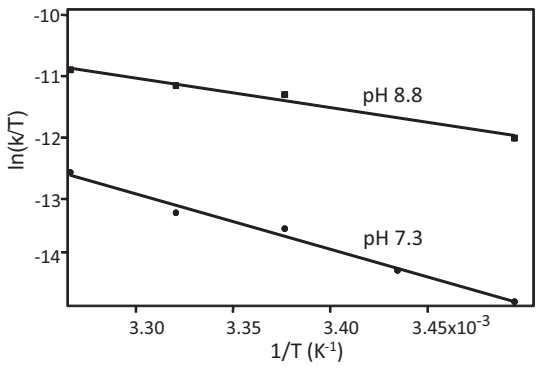

Fig 10. Eyring plots of the H/D exchange reaction at pH 7.3 and 8.8. The parameters, determined from a linear fit of the data, are listed in Table 1.

Table 1
Thermodynamic parameters associated with the H/D exchange reaction near the propionate groups of heme *a* in bCcO.

Activation parameters	pH 7.3	pH 8.8
$\Delta H^{\ddagger}$ (kcal mol^{-1})	18.0	7.1
$T\Delta S^{\ddagger}$ (kcal mol^{-1})	−4.1	−13.5
$\Delta G^{\ddagger}$ (kcal mol^{-1})	22.1	20.6

described in Section 3.4. The new data reported here confirm that rapid H/D exchange occurs near the propionate groups of heme a_3, whereas exchange near heme *a* is detected when heme *a* is oxidized but not when it is reduced.

Under all conditions, rapid proton exchange near the heme a_3 propionates was observed. As illustrated in Figs. 3 and 11, there is a large cluster of water molecules associated with the heme a_3 propionates which, as pointed out by Tiefenbrunn et al., is a common feature of terminal oxidases spanning many diverse species, supporting its functional importance [75]. This cluster leads to the Mg ion, part of the putative route for the pumped protons, and from there along polar channels containing water molecules to the P-side of the membrane. One potential pathway is depicted in Fig. 11, in which a channel is formed by a large number of crystallographically identified water molecules. It should be noted that this water channel, as well as two others, have been identified by Sugitani and Stuchebrukhov, through which water molecules formed at the binuclear center, as well as pumped protons, could exit the protein [20]. However, as noted previously [19], it has been postulated that this pathway does not allow reverse proton translocation. If reverse proton translocation cannot occur through this pathway, then access to the propionates of heme a_3 would have to pass through the K or D pathways. Thus, one or more of these pathways could be conduits for proton entry to the region near the propionate groups of heme a_3, accounting for the rapid exchange detected in the propionate groups of heme a_3.

As heme *a* is embedded in the protein, proton access to it must also pass through the polypeptide *via* a channel of labile groups. Based on crystal structure data, there are two potential pathways for protons to reach the heme *a* propionate region from outside the membrane. The first potential pathway is the H-channel proposed previously by Yoshikawa and coworkers [3]. The H-channel, illustrated in Fig. 12, originates near H413, on the N-side of the membrane, passes near the

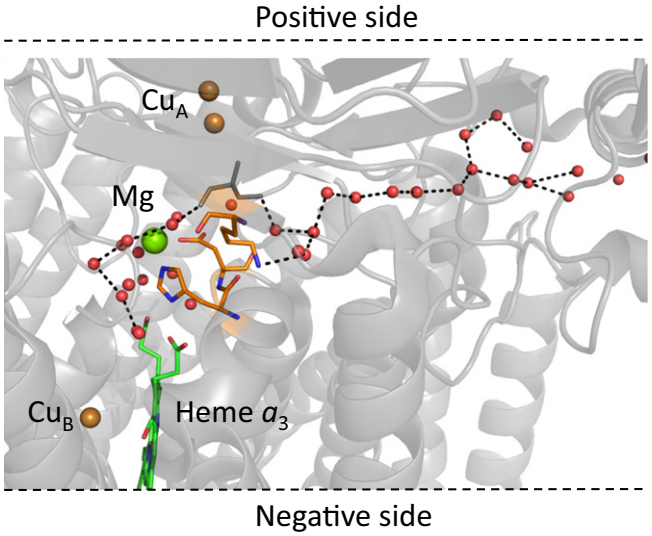

Fig. 11. A putative proton exchange pathway connecting the heme a_3 propionate groups to the P-side of the membrane (PDB: 3ABL). A series of crystallographically identified water molecules link the cluster of waters near the heme a_3 propionate groups *via* the magnesium ion to the P-side of the membrane. The water molecules (red spheres) are separated by ~2.7–3.3 Å.

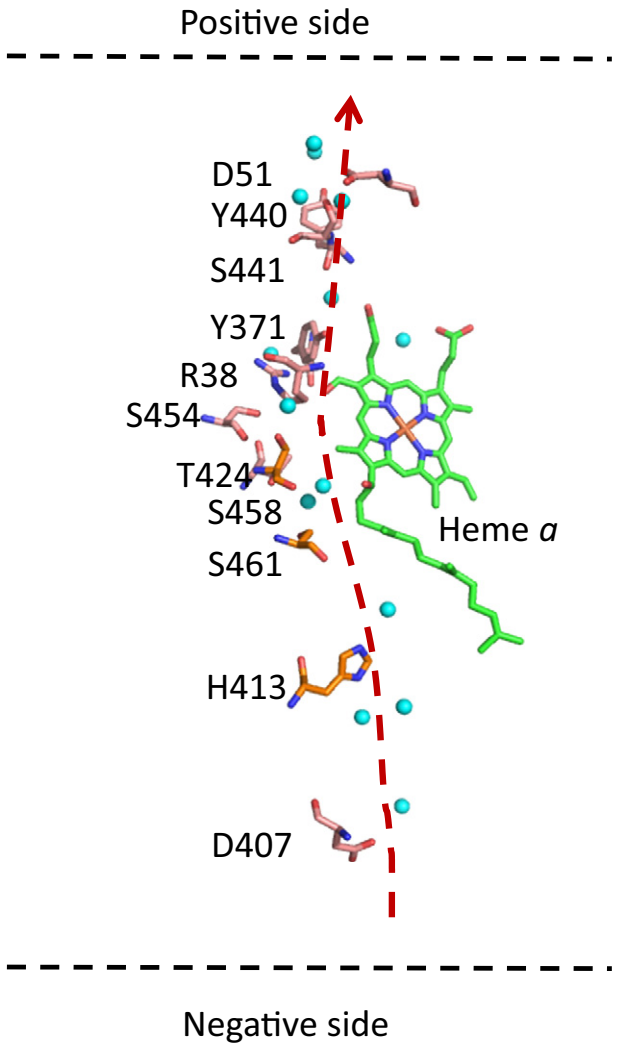

Fig. 12. Critical residues and water molecules (blue spheres) comprising the H-channel.

edge of heme *a* along the A-ring propionate group, and exits at D51 on the P-side of the membrane.

To evaluate this pathway, we calculated the pK_a of each of the labile amino acid residues lining the H-pathway in oxidized bCcO by an empirical pK_a calculation program (PROPKA 3.1, Web version) [76]. Intriguingly, although the apparent pK_a we determined for the H/D exchange reaction is ~8.0, none of these residues had a pK_a near 8.0 (the calculated pK_a values were at least 3 pH units higher or lower from 8.0; data not shown). However, the calculations may not properly account for the role of the water molecules in the pathway. It is generally assumed that passage through the H-pathway, as well as the other pathways, occurs *via* the Grotthuss mechanism, in which one proton enters at the channel entrance and another one leaves at the exit point in a dynamic process governed by Brownian ratchet diffusive motion [77,78]. This is an oversimplification as several factors must be considered, such as the pK_a's of the donors and acceptors [79], the electrostatic expense of removing a proton from the aqueous environment [80], and the re-orientation of the labile groups in the pathway to reset the channel [81]. Due to the complexity, it is difficult to firmly assign the apparent pK_a (8.0) to a specific residue for the H/D exchange reaction. However, it is noteworthy that a similar pK_a has been identified in the past in photodissociation experiments [13,14,64]. In those experiments, frequency shifts and intensity changes were seen in the 1730–1750 cm^{-1} spectral window, following photodissociation of CO from heme a_3 in the mixed valence enzyme. Although there is no consensus on the assignments of the residue(s) associated with the changes, the modes no doubt originate from carboxylic acid groups. Furthermore, due to the reverse electron transfer from heme a_3 to heme *a* that occurs following CO photodissociation in the mixed valence enzyme, the changes may be induced by a change in the redox state of heme *a*, consistent with the observations reported here.

The second potential pathway for protons to reach the heme *a* propionate region is mediated by the water cluster near the heme a_3 propionates [75]. As noted above, there is rapid access to the propionate region near heme a_3, in contrast to the slow proton access to the propionate region near heme *a* [5]. It has been postulated that the proton transfer between heme *a* and heme a_3 is blocked by the two arginine residues that form salt bridges with the propionates of the two heme groups [5]. However, it is possible that pH dependent changes of these residues could open a pathway and allow access of protons to the heme *a* propionate groups. This scenario is supported by a 3 Å resolution structure of *P. denitrificans* CcO by Michel and coworkers [82], obtained at pH 8, which revealed a change in the position of R474 (R439 in bCcO) as compared to its conserved position in the other reported structures obtained at lower pH values (see Fig. 13). In this unique position, R474 is rotated ~90°, and it has a different H-bonding pattern as compared to the equivalent Arg in other structures. This change in orientation could possibly eliminate the blockage, allowing proton access to the heme *a* propionate region.

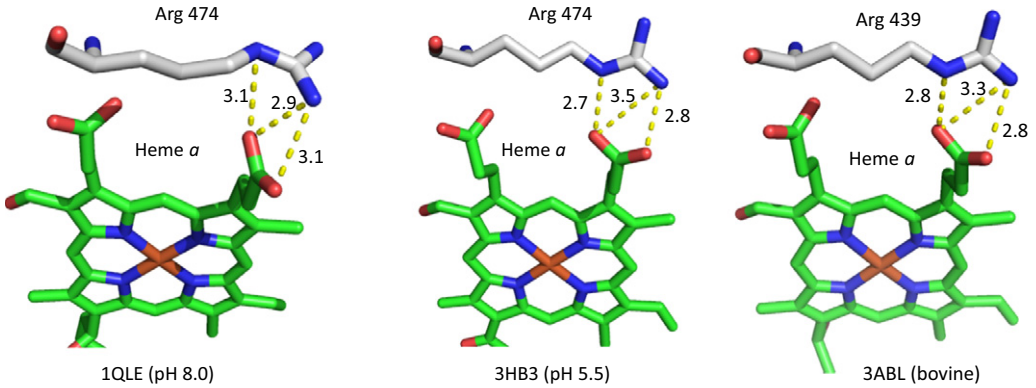

Fig. 13. Comparison of the H-bonding interactions between R474 and the D-ring propionate group of heme *a* in *P. denitrificans* CcO at pH 8.0 (PDB: 1QLE) and pH 5.5 (PDB: 3HB3) and the equivalent interactions involving R439 in bovine CcO (PDB: 3ABL).

To further test this hypothesis, we used PROPKA 3.1 [76] to calculate the pK_a's of the two Arg residues that H-bond to the heme propionate groups in bCcO (R438 and R439) and in *P. denitrificans* CcO (R473 and R474). The pK_a of R438 in several available structures of bCcO was determined to be between 15.5 and 16.0, while that of R439 was determined to be between 12.8 and 13.1, much higher than our detected pK_a for the H/D exchange of 8.0. Likewise, the pK_a's of the two Arg residues in the structure of *P. denitrificans* CcO crystallized at pH 5.5 were found to be similar to those of bCcO. However, those in the structure crystallized at pH 8 (1QLE) have much lower pK_a's (9.0 and 11.5 for R473 and R474, respectively). These differences are attributed to the large difference in the H-bonding network of the Arg residues (Fig. 13). To our knowledge, the *P. denitrificans* structure referred to above is the only reported structure that was obtained at pH 8. Additional studies are required to determine if bCcO could adopt a similar conformation at high pH, and if such conformational changes could account for the apparent pK_a observed in the H/D exchange reaction associated with heme *a*.

Temperature-dependent studies of the H/D exchange reaction showed that the increase of pH from 7.3 to 8.8 leads to a change in the activation enthalpy and entropy by factors of >2 (Table 1), but minimal change was observed in the activation free energy, manifesting a significant enthalpy–entropy compensation [74]. The observed higher enthalpic barrier (by ~11 kcal/mol), at pH 7.3 compared to 8.8, is equivalent to the energy of a few H-bonds, suggesting that to overcome the transition state barrier for the H/D exchange reaction requires the breakage of a few additional H-bonds. In contrast, at pH 8.8, the enthalpic barrier is lower, while the activation entropic barrier is ~9 kcal/mol higher indicating that although fewer H-bonds have to be broken, the reaction has to overcome a higher conformational barrier, possibly due to the loss of H-bonds at high pH. The data reveal that at neutral pH, the H/D exchange reaction is limited by an enthalpic barrier — the breakage of H-bonds between the critical residues, water molecules and/or the proton loading site, while the increase in pH leads to a new mechanism that is limited by an entropic barrier — the conformational rearrangement of residues/water molecules in the proton pathway and/or loading site.

In general, the data reported here confirm the ability of protons to access the propionate regions of heme *a* and heme a_3 under equilibrium conditions. They support a previously proposed model that the propionates of heme *a* are part of the proton loading site that is linked to the N-side of the membrane *via* the H-channel [5]. Additional experiments on bacterial oxidases are needed to determine if the H/D exchange properties reported here are unique to the bovine CcO.

5. Conclusions

Until we are able to determine the structure of each catalytic intermediate of cytochrome *c* oxidase populated during the catalytic reaction, vibrational spectroscopy remains a powerful technique for probing the mechanism by which the oxygen reduction reaction is coupled to proton translocation. The coupling of vibrational spectroscopy with H/D exchange methods, as well as infrared difference spectroscopy and advanced time-resolved infrared and Raman spectroscopies, have shown great utility in revealing important structural features associated with proton translocation. In addition, over the past several years, the resolution of the crystal structures of cytochrome oxidases has been steadily improving and is approaching the atomic level, which will allow the identification of proton locations in equilibrium states of the enzymes. A recent and very exciting advance in crystallography is the use of the X-ray free-electron laser (XFEL) as the light source. This new technology has been applied to structural analysis of bCcO, permitting detailed determination of the crystal structure of the oxidized enzyme without the complication derived from photo-induced reduction of the enzymes by the X-ray beam [83]. The next foreseeable step is to combine time-resolved methodology [84] with the XFEL to determine the crystal structure of each of the catalytic intermediates identified by vibrational and optical absorption spectroscopies, and to carry out comparable studies of enzymes isolated from differing species. It is anticipated that the combination of these results with vibrational studies will resolve the proton translocation mechanism and answer the question of whether or not there is a common mechanism shared by the enzymes from the various organisms.

Acknowledgements

This work was supported the National Institutes of Health grants GM098799 to D.L.R., and GM086482 to S.-R.Y.

References

[1] S. Yoshikawa, K. Muramoto, K. Shinzawa-Itoh, Proton-pumping mechanism of cytochrome *c* oxidase, Annu. Rev. Biophys. 40 (2011) 205–223.
[2] I. Belevich, M.I. Verkhovsky, Molecular mechanism of proton translocation by cytochrome *c* oxidase, Antioxid. Redox Signal. 10 (2008) 1–29.
[3] T. Tsukihara, K. Shimokata, Y. Katayama, H. Shimada, K. Muramoto, H. Aoyama, M. Mochizuki, K. Shinzawa-Itoh, E. Yamashita, M. Yao, Y. Ishimura, S. Yoshikawa, The low-spin heme of cytochrome *c* oxidase as the driving element of the proton-pumping process, Proc. Natl. Acad. Sci. U. S. A. 100 (2003) 15304–15309.
[4] T. Egawa, H.J. Lee, H. Ji, R.B. Gennis, S.R. Yeh, D.L. Rousseau, Identification of heme propionate vibrational modes in the resonance Raman spectra of cytochrome *c* oxidase, Anal. Biochem. 394 (2009) 141–143.
[5] T. Egawa, S.R. Yeh, D.L. Rousseau, Redox-controlled proton gating in bovine cytochrome *c* oxidase, PLoS ONE 8 (2013) e63669.
[6] R.B. Gennis, Some recent contributions of FTIR difference spectroscopy to the study of cytochrome oxidase, FEBS Lett. 555 (2003) 2–7.
[7] J. Behr, P. Hellwig, W. Mantele, H. Michel, Redox dependent changes at the heme propionates in cytochrome *c* oxidase from *Paracoccus denitrificans*: direct evidence from FTIR difference spectroscopy in combination with heme propionate 13C labeling, Biochemistry 37 (1998) 7400–7406.
[8] J. Behr, H. Michel, W. Mantele, P. Hellwig, Functional properties of the heme propionates in cytochrome *c* oxidase from *Paracoccus denitrificans*. Evidence from FTIR difference spectroscopy and site-directed mutagenesis, Biochemistry 39 (2000) 1356–1363.
[9] P. Hellwig, A. Bohm, U. Pfitzner, W. Mantele, B. Ludwig, Spectroscopic study on the communication between a heme a3 propionate, Asp399 and the binuclear center of cytochrome *c* oxidase from *Paracoccus denitrificans*, Biochim. Biophys. Acta 1777 (2008) 220–226.
[10] P. Hellwig, S. Grzybek, J. Behr, B. Ludwig, H. Michel, W. Mantele, Electrochemical and ultraviolet/visible/infrared spectroscopic analysis of heme a and a3 redox reactions in the cytochrome *c* oxidase from *Paracoccus denitrificans*: separation of heme a and a3 contributions and assignment of vibrational modes, Biochemistry 38 (1999) 1685–1694.
[11] P. Hellwig, U. Pfitzner, J. Behr, B. Rost, R.P. Pesavento, W.V. Donk, R.B. Gennis, H. Michel, B. Ludwig, W. Mantele, Vibrational modes of tyrosines in cytochrome *c* oxidase from *Paracoccus denitrificans*: FTIR and electrochemical studies on Tyr-D4-labeled and on Tyr280His and Tyr35Phe mutant enzymes, Biochemistry 41 (2002) 9116–9125.
[12] M. Iwaki, A. Puustinen, M. Wikstrom, P.R. Rich, Structural and chemical changes of the P(M) intermediate of *Paracoccus denitrificans* cytochrome *c* oxidase revealed by IR spectroscopy with labeled tyrosines and histidine, Biochemistry 45 (2006) 10873–10885.
[13] B.H. McMahon, M. Fabian, F. Tomson, T.P. Causgrove, J.A. Bailey, F.N. Rein, R.B. Dyer, G. Palmer, R.B. Gennis, W.H. Woodruff, FTIR studies of internal proton transfer reactions linked to inter-heme electron transfer in bovine cytochrome *c* oxidase, Biochim. Biophys. Acta 1655 (2004) 321–331.
[14] D. Okuno, T. Iwase, K. Shinzawa-Itoh, S. Yoshikawa, T. Kitagawa, FTIR detection of protonation/deprotonation of key carboxyl side chains caused by redox change of the Cu(A)–heme *a* moiety and ligand dissociation from the heme a_3–Cu(B) center of bovine heart cytochrome *c* oxidase, J. Am. Chem. Soc. 125 (2003) 7209–7218.
[15] P.R. Rich, J. Breton, FTIR studies of the CO and cyanide adducts of fully reduced bovine cytochrome *c* oxidase, Biochemistry 40 (2001) 6441–6449.
[16] T. Uchida, T. Mogi, H. Nakamura, T. Kitagawa, Role of Tyr-288 at the dioxygen reduction site of cytochrome *bo* studied by stable isotope labeling and resonance Raman spectroscopy, J. Biol. Chem. 279 (2004) 53613–53620.
[17] M. Kubo, S. Nakashima, S. Yamaguchi, T. Ogura, M. Mochizuki, J. Kang, M. Tateno, K. Shinzawa-Itoh, K. Kato, S. Yoshikawa, Effective pumping proton collection facilitated by a copper site (CuB) of bovine heart cytochrome *c* oxidase, revealed by a newly developed time-resolved infrared system, J. Biol. Chem. 288 (2013) 30259–30269.
[18] V.R. Kaila, V. Sharma, M. Wikstrom, The identity of the transient proton loading site of the proton-pumping mechanism of cytochrome *c* oxidase, Biochim. Biophys. Acta 1807 (2011) 80–84.
[19] D.M. Popovic, A.A. Stuchebrukhov, Proton exit channels in bovine cytochrome *c* oxidase, J. Phys. Chem. B 109 (2005) 1999–2006.
[20] R. Sugitani, A.A. Stuchebrukhov, Molecular dynamics simulation of water in cytochrome *c* oxidase reveals two water exit pathways and the mechanism of transport, Biochim. Biophys. Acta 1787 (2009) 1140–1150.
[21] Y. Song, E. Michonova-Alexova, M.R. Gunner, Calculated proton uptake on anaerobic reduction of cytochrome *c* oxidase: is the reaction electroneutral? Biochemistry 45 (2006) 7959–7975.

[22] R.M. Nyquist, D. Heitbrink, C. Bolwien, T.A. Wells, R.B. Gennis, J. Heberle, Perfusion-induced redox differences in cytochrome *c* oxidase: ATR/FT-IR spectroscopy, FEBS Lett. 505 (2001) 63–67.
[23] P.R. Rich, J. Breton, Attenuated total reflection Fourier transform infrared studies of redox changes in bovine cytochrome *c* oxidase: resolution of the redox Fourier transform infrared difference spectrum of heme a(3), Biochemistry 41 (2002) 967–973.
[24] I. Ishigami, T. Nishigaki, K. Shinzawa-Itoh, S. Yoshikawa, S. Nakashima, T. Ogura, An intermediate conformational state during ligand binding to cytochrome *c* oxidase detected by time-resolved resonance Raman analyses of heme peripheral groups, Chem. Lett. 41 (2012) 178–180.
[25] D.L. Rousseau, S. Han, Time-resolved resonance Raman spectroscopy of intermediates in cytochrome oxidase, Methods Enzymol. 354 (2002) 351–368.
[26] T. Ogura, S. Takahashi, S. Hirota, K. Shinzawa-Itoh, S. Yoshikawa, E.H. Appelman, T. Kitagawa, Time-resolved resonance Raman elucidation of the pathway for dioxygen reduction by cytochrome *c* oxidase, J. Am. Chem. Soc. 115 (1993) 8527–8536.
[27] G.T. Babcock, C. Varotsis, Discrete steps in dioxygen activation—the cytochrome oxidase/O_2 reaction, J. Bioenerg. Biomembr. 25 (1993) 71–80.
[28] S. Han, Y.C. Ching, D.L. Rousseau, Ferryl and hydroxy intermediates in the reaction of oxygen with reduced cytochrome *c* oxidase, Nature 348 (1990) 89–90.
[29] S. Han, S. Takahashi, D.L. Rousseau, Time dependence of the catalytic intermediates in cytochrome *c* oxidase, J. Biol. Chem. 275 (2000) 1910–1919.
[30] T. Kitagawa, Structures of reaction intermediates of bovine cytochrome *c* oxidase probed by time-resolved vibrational spectroscopy, J. Inorg. Biochem. 82 (2000) 9–18.
[31] T. Kitagawa, T. Ogura, Time-resolved resonance Raman investigation of oxygen reduction mechanism of bovine cytochrome *c* oxidase, J. Bioenerg. Biomembr. 30 (1998) 71–79.
[32] C. Varotsis, Y. Zhang, E.H. Appelman, G.T. Babcock, Resolution of the reaction sequence during the reduction of O_2 by cytochrome oxidase, Proc. Natl. Acad. Sci. U. S. A. 90 (1993) 237–241.
[33] C. Varotsis, W.H. Woodruff, G.T. Babcock, Direct detection of a dioxygen adduct of cytochrome a_3 in the mixed valence cytochrome oxidase/dioxygen reaction, J. Biol. Chem. 265 (1990) 11131–11136.
[34] G.T. Babcock, J.M. Jean, L.N. Johnston, W.H. Woodruff, G. Palmer, Flow-flash, time-resolved resonance Raman spectroscopy of the oxidation of reduced and of mixed valence cytochrome oxidase by dioxygen, J. Inorg. Biochem. 23 (1985) 243–251.
[35] S. Han, Y.C. Ching, D.L. Rousseau, Primary intermediate in the reaction of mixed-valence cytochrome *c* oxidase with oxygen, Biochemistry 29 (1990) 1380–1384.
[36] S.W. Han, Y.C. Ching, D.L. Rousseau, Primary intermediate in the reaction of oxygen with fully reduced cytochrome *c* oxidase, Proc. Natl. Acad. Sci. U. S. A. 87 (1990) 2491–2495.
[37] D.A. Proshlyakov, T. Ogura, K. Shinzawa-Itoh, S. Yoshikawa, E.H. Appelman, T. Kitagawa, Selective resonance Raman observation of the "607 nm" form generated in the reaction of oxidized cytochrome *c* oxidase with hydrogen peroxide, J. Biol. Chem. 269 (1994) 29385–29388.
[38] M. Fabian, W.W. Wong, R.B. Gennis, G. Palmer, Mass spectrometric determination of dioxygen bond splitting in the "peroxy" intermediate of cytochrome *c* oxidase, Proc. Natl. Acad. Sci. U. S. A. 96 (1999) 13114–13117.
[39] M. Fabian, G. Palmer, The interaction of cytochrome oxidase with hydrogen peroxide: the relationship of compounds **P** and **F**, Biochemistry 34 (1995) 13802–13810.
[40] D.A. Proshlyakov, M.A. Pressler, G.T. Babcock, Dioxygen activation and bond cleavage by mixed-valence cytochrome *c* oxidase, Proc. Natl. Acad. Sci. U. S. A. 95 (1998) 8020–8025.
[41] E. Pinakoulaki, V. Daskalakis, T. Ohta, O.M. Richter, K. Budiman, T. Kitagawa, B. Ludwig, C. Varotsis, The protein effect in the structure of two ferryl-oxo intermediates at the same oxidation level in the heme copper binuclear center of cytochrome *c* oxidase, J. Biol. Chem. 288 (2013) 20261–20266.
[42] C. Varotsis, G.T. Babcock, Appearance of the ν(FeIV═O) vibration from a ferryl-oxo intermediate in the cytochrome oxidase/dioxygen reaction, Biochemistry 29 (1990) 7357–7362.
[43] R. Mitchell, P.R. Rich, Proton uptake by cytochrome *c* oxidase on reduction and on ligand binding, Biochim. Biophys. Acta 1186 (1994) 19–26.
[44] Y.C. Kim, M. Wikstrom, G. Hummer, Kinetic gating of the proton pump in cytochrome *c* oxidase, Proc. Natl. Acad. Sci. U. S. A. 106 (2009) 13707–13712.
[45] V.R. Kaila, M.I. Verkhovsky, G. Hummer, M. Wikstrom, Glutamic acid 242 is a valve in the proton pump of cytochrome *c* oxidase, Proc. Natl. Acad. Sci. U. S. A. 105 (2008) 6255–6259.
[46] T. Yamashita, G.A. Voth, Insights into the mechanism of proton transport in cytochrome *c* oxidase, J. Am. Chem. Soc. 134 (2012) 1147–1152.
[47] V.R. Kaila, M.I. Verkhovsky, G. Hummer, M. Wikstrom, Mechanism and energetics by which glutamic acid 242 prevents leaks in cytochrome *c* oxidase, Biochim. Biophys. Acta 1787 (2009) 1205–1214.
[48] A.L. Woelke, G. Galstyan, A. Galstyan, T. Meyer, J. Heberle, E.W. Knapp, Exploring the possible role of Glu286 in CcO by electrostatic energy computations combined with molecular dynamics, J. Phys. Chem. B 117 (2013) 12432–12441.
[49] J. Koepke, E. Olkhova, H. Angerer, H. Muller, G. Peng, H. Michel, High resolution crystal structure of *Paracoccus denitrificans* cytochrome *c* oxidase: new insights into the active site and the proton transfer pathways, Biochim. Biophys. Acta 1787 (2009) 635–645.
[50] M.A. Sharpe, S. Ferguson-Miller, A chemically explicit model for the mechanism of proton pumping in heme-copper oxidases, J. Bioenerg. Biomembr. 40 (2008) 541–549.
[51] M. Wikstrom, M.I. Verkhovsky, Mechanism and energetics of proton translocation by the respiratory heme–copper oxidases, Biochim. Biophys. Acta 1767 (2007) 1200–1214.
[52] K. Faxen, G. Gilderson, P. Adelroth, P. Brzezinski, A mechanistic principle for proton pumping by cytochrome *c* oxidase, Nature 437 (2005) 286–289.
[53] S.A. Siletsky, A.A. Konstantinov, Cytochrome *c* oxidase: charge translocation coupled to single-electron partial steps of the catalytic cycle, Biochim. Biophys. Acta 1817 (2012) 476–488.
[54] M. Wikstrom, M.I. Verkhovsky, G. Hummer, Water-gated mechanism of proton translocation by cytochrome *c* oxidase, Biochim. Biophys. Acta 1604 (2003) 61–65.
[55] P. Brzezinski, R.B. Gennis, Cytochrome *c* oxidase: exciting progress and remaining mysteries, J. Bioenerg. Biomembr. 40 (2008) 521–531.
[56] P.R. Rich, A. Marechal, Functions of the hydrophilic channels in protonmotive cytochrome *c* oxidase, J. R. Soc. Interface. 10 (2013) 20130183.
[57] A. Tuukkanen, V.R. Kaila, L. Laakkonen, G. Hummer, M. Wikstrom, Dynamics of the glutamic acid 242 side chain in cytochrome *c* oxidase, Biochim. Biophys. Acta 1767 (2007) 1102–1106.
[58] S. Papa, N. Capitanio, G. Villani, A cooperative model for protonmotive heme–copper oxidases. The role of heme a in the proton pump of cytochrome *c* oxidase, FEBS Lett. 439 (1998) 1–8.
[59] P. Goyal, J. Lu, S. Yang, M.R. Gunner, Q. Cui, Changing hydration level in an internal cavity modulates the proton affinity of a key glutamate in cytochrome *c* oxidase, Proc. Natl. Acad. Sci. U. S. A. 110 (2013) 18886–18891.
[60] P. Hellwig, B. Rost, U. Kaiser, C. Ostermeier, H. Michel, W. Mantele, Carboxyl group protonation upon reduction of the *Paracoccus denitrificans* cytochrome *c* oxidase: direct evidence by FTIR spectroscopy, FEBS Lett. 385 (1996) 53–57.
[61] P. Hellwig, J. Behr, C. Ostermeier, O.M. Richter, U. Pfitzner, A. Odenwald, B. Ludwig, H. Michel, W. Mantele, Involvement of glutamic acid 278 in the redox reaction of the cytochrome *c* oxidase from *Paracoccus denitrificans* investigated by FTIR spectroscopy, Biochemistry 37 (1998) 7390–7399.
[62] A. Puustinen, J.A. Bailey, R.B. Dyer, S.L. Mecklenburg, M. Wikstrom, W.H. Woodruff, Fourier transform infrared evidence for connectivity between CuB and glutamic acid 286 in cytochrome bo_3 from *Escherichia coli*, Biochemistry 36 (1997) 13195–13200.
[63] R.M. Nyquist, D. Heitbrink, C. Bolwien, R.B. Gennis, J. Heberle, Direct observation of protonation reactions during the catalytic cycle of cytochrome *c* oxidase, Proc. Natl. Acad. Sci. U. S. A. 100 (2003) 8715–8720.
[64] M. Iwaki, P.R. Rich, An IR study of protonation changes associated with heme–heme electron transfer in bovine cytochrome *c* oxidase, J. Am. Chem. Soc. 129 (2007) 2923–2929.
[65] S. Yang, Q. Cui, Glu-286 rotation and water wire reorientation are unlikely the gating elements for proton pumping in cytochrome *c* oxidase, Biophys. J. 101 (2011) 61–69.
[66] M.A. Yu, T. Egawa, K. Shinzawa-Itoh, S. Yoshikawa, V. Guallar, S.R. Yeh, D.L. Rousseau, G.J. Gerfen, Two tyrosyl radicals stabilize high oxidation states in cytochrome *c* oxidase for efficient energy conservation and proton translocation, J. Am. Chem. Soc. 134 (2012) 4753–4761.
[67] M.A. Yu, T. Egawa, K. Shinzawa-Itoh, S. Yoshikawa, S.R. Yeh, D.L. Rousseau, G.J. Gerfen, Radical formation in cytochrome *c* oxidase, Biochim. Biophys. Acta 1807 (2011) 1295–1304.
[68] O. Einarsdottir, R.B. Dyer, D.D. Lemon, P.M. Killough, S.M. Hubig, S.J. Atherton, J.J. Lopez-Garriga, G. Palmer, W.H. Woodruff, Photodissociation and recombination of carbonmonoxy cytochrome oxidase: dynamics from picoseconds to kiloseconds, Biochemistry 32 (1993) 12013–12024.
[69] K. Kamiya, M. Boero, M. Tateno, K. Shiraishi, A. Oshiyama, Possible mechanism of proton transfer through peptide groups in the H-pathway of the bovine cytochrome *c* oxidase, J. Am. Chem. Soc. 129 (2007) 9663–9673.
[70] K. Shimokata, Y. Katayama, H. Murayama, M. Suematsu, T. Tsukihara, K. Muramoto, H. Aoyama, S. Yoshikawa, H. Shimada, The proton pumping pathway of bovine heart cytochrome *c* oxidase, Proc. Natl. Acad. Sci. U. S. A. 104 (2007) 4200–4205.
[71] S. Yoshikawa, M.G. Choc, M.C. O'toole, W.S. Caughey, An infrared study of CO binding to heart cytochrome *c* oxidase and hemoglobin A. Implications re O_2 reactions. J. Biol. Chem. 252 (1977) 5498–5508.
[72] X. Hu, H. Frei, T.G. Spiro, Nanosecond step-scan FTIR spectroscopy of hemoglobin: ligand recombination and protein conformational changes, Biochemistry 35 (1996) 13001–13005.
[73] X.-Y. Li, R.S. Czernuszewicz, J.R. Kincaid, P. Stein, T.G. Spire, Consistent porphyrin force field. 2. Nickel octaethylporphyrin skeletal and substituent mode assignments from 15N, meso-d4, and methylene-d, Raman and infrared isotope shifts, J. Phys. Chem. 94 (1990) 47–61.
[74] J.D. Dunitz, Win some, lose some: enthalpy-entropy compensation in weak intermolecular interactions, Chem. Biol. 2 (1995) 709–712.
[75] T. Tiefenbrunn, W. Liu, Y. Chen, V. Katritch, C.D. Stout, J.A. Fee, V. Cherezov, High resolution structure of the ba^3 cytochrome *c* oxidase from *Thermus thermophilus* in a lipidic environment, PLoS ONE 6 (2011) e22348.
[76] H. Li, A.D. Robertson, J.H. Jensen, Very fast empirical prediction and rationalization of protein pK_a values, Proteins 61 (2005) 704–721.
[77] N. Agmon, The Grotthuss mechanism, Chem. Phys. Lett. 244 (1995) 456–462.
[78] R. Pomès, Theoretical studies of the Grotthuss mechanism in biological proton wires, Israel J. Chem. 39 (1999) 387–395.
[79] C.A. Wraight, Chance and design–proton transfer in water, channels and bioenergetic proteins, Biochim. Biophys. Acta 1757 (2006) 886–912.
[80] A. Burykin, A. Warshel, What really prevents proton transport through aquaporin? Charge self-energy versus proton wire proposals, Biophys. J. 85 (2003) 3696–3706.
[81] J.F. Nagle, S. Tristram-Nagle, Hydrogen bonded chain mechanisms for proton conduction and proton pumping, J. Membr. Biol. 74 (1983) 1–14.
[82] A. Harrenga, H. Michel, The cytochrome *c* oxidase from *Paracoccus denitrificans* does not change the metal center ligation upon reduction, J. Biol. Chem. 274 (1999) 33296–33299.
[83] K. Hirata, K. Shinzawa-Itoh, N. Yano, S. Takemura, K. Kato, M. Hatanaka, K. Muramoto, T. Kawahara, T. Tsukihara, E. Yamashita, K. Tono, G. Ueno, T. Hikima, H. Murakami, Y. Inubushi, M. Yabashi, T. Ishikawa, M. Yamamoto, T. Ogura, H. Sugimoto, J.R. Shen, S. Yoshikawa, H. Ago, Determination of damage-free crystal structure of an X-ray-sensitive protein using an XFEL, Nat. Methods 11 (2014) 734–736.
[84] A. Barty, J. Kupper, H.N. Chapman, Molecular imaging using X-ray free-electron lasers, Annu. Rev. Phys. Chem. 64 (2013) 415–435.